INSTITUTE OF PHYSICS PUBLISHING JOURNAL OF OPTICS B: QUANTUM AND SEMICLASSICAL OPTICS

J. Opt. B: Quantum Semiclass. Opt. **5** (2003) 129–137 PII: S1464-4266(03)56452-7

Cavity-quantum electrodynamics with quantum dots

A Kiraz[1,2], C Reese[1], B Gayral[1,3], Lidong Zhang[1], W V Schoenfeld[1], B D Gerardot[1], P M Petroff[1], E L Hu[1] and A Imamoğlu[1,4,5]

[1] Departments of Electrical and Computer Engineering, Materials, and Physics, University of California, Santa Barbara, CA 93106, USA
[2] Department Chemie, Ludwig-Maximilians Universität München, Butenandtstrasse 11, D-81377 München, Germany
[3] Schlumberger EPS-SRPC, 1 rue Becquerel, 92142 Clamart, France
[4] Faculty of Engineering and Natural Sciences, Sabanci University, Istanbul, Turkey
[5] Institute of Quantum Electronics, ETH-Honggerberg HPT G10.2, CH-8093 Zurich, Switzerland

Received 11 November 2002, in final form 7 February 2003
Published 27 February 2003
Online at stacks.iop.org/JOptB/5/129

Abstract
Semiconductor quantum dots (QDs) have emerged as promising candidates for studying quantum optical phenomena. In particular, cavity-quantum electrodynamics effects can be investigated using a single QD embedded inside a photonic nanostructure, where both the carriers and photons are confined within sub-micron length scales in all three dimensions. Since QD location inside the cavity is fixed by the growth, this system is free of the stringent trapping requirements that limit its atomic counterpart. The possibility of fabricating photonic nanostructures with ultra-small optical-mode volumes and long photon lifetimes enhances the prospects for applications in quantum information processing.

Keywords: Cavity-QED, quantum dot, Purcell effect, microdisc, photonic crystal, photonic band gap

(Some figures in this article are in colour only in the electronic version)

1. Introduction

The elementary system in cavity-quantum electrodynamics (QED) is a two-level emitter interacting resonantly with a single cavity mode. Basic properties of the two-level emitter can be dramatically modified if the photon lifetime, determined by the cavity quality (Q) factor, is long, and the electric field per photon (E_{vac}) inside the cavity, determined by the square root of the reciprocal cavity volume (V_{cav}), is large. Since the 1980s, several experiments have demonstrated that radiative decay rate can be significantly modified by placing atoms inside a cavity structure [1]. The enhancement (Purcell) factor, defined as the ratio of the spontaneous emission rate inside the cavity to that in free-space, is proportional to Q/V_{cav} and is independent of the atomic parameters such as the dipole matrix element. If the cavity has a preferential output direction, the Purcell effect will ensure fast and directional emission from the two-level system. These features are highly desirable for applications in optoelectronics as well as in quantum information science.

If E_{vac} is sufficiently large, then the energy exchange between the two-level system and the cavity mode will be reversible. To attain this so-called strong-coupling regime of cavity-QED, the single-photon Rabi frequency $g \propto E_{vac}$ must exceed the decoherence rates in the composite system originating from photon losses (Γ_{cav}) determined by the cavity quality factor and dipole dephasing (Γ_{deph}) ultimately determined by the spontaneous emission rate. Experiments based on a single atom injected into a high-Q cavity have achieved the strong-coupling regime of cavity-QED, which in turn enabled the demonstration of conditional quantum dynamics [2], decoherence of mesoscopic superposition of quantum states and creation of entanglement between three distinguishable quantum systems [3]. In most cases, these experiments are limited by the difficulty in trapping a single atom at an anti-node of the cavity mode. For optical cavities, there is an additional limitation arising from the fact that typical cavity volumes are approximately 10^4 times larger than the fundamental limit for photon confinement given by $(\lambda/2n)^3$.

In contrast, quantum dots (QDs) embedded in photonic nanostructures overcome these difficulties in a natural way. QDs are structures in which electron motion is confined in all three dimensions. Since confinement leads to a discrete energy spectrum, QDs are sometimes referred to as artificial atoms. On the other hand, the confinement length-scale of electrons in QDs extends over many lattice sites, giving rise to physical phenomena that are distinct from their atomic counterparts. Of particular interest in photonics are semiconductor QD structures that confine both electron and hole motion, resulting in a discrete optical excitation spectra. The optical excitations in such QDs are collective in nature and exhibit oscillator strengths that can exceed 100, even though the spectrum is strongly anharmonic [4].

The goal of this paper is to provide a review of recent results we have obtained using self-assembled InAs QDs coupled to either microdisc or two-dimensional (2D) photonic crystal defect cavities. After a brief overview of the state-of-the-art in section 2, we discuss experiments demonstrating the Purcell effect for a single QD coupled to a single microdisc cavity mode in section 3. In section 4, we concentrate on the observation of high quality factor photonic crystal defect modes. We discuss techniques to control QD nucleation and to maximize QD–cavity coupling in sections 5 and 6, respectively. We conclude by discussing potential applications of QD cavity-QED in quantum information processing (QIP) (section 7).

2. Review of quantum dots and photonic nanostructures

Key elements of QD cavity-QED systems are self-assembled InAs QDs grown by molecular beam epitaxy (MBE), and semiconductor optical nano-cavities that contain embedded QDs. Self-assembled QD islands form spontaneously during MBE growth due to the lattice mismatch between two semiconductors. During growth, the total film energy, including strain energy, interfacial energy and surface energy, will be minimized through the formation of coherently strained islands. The direct crystal growth of self-assembling QDs has been widely recognized as one of the easiest approaches for forming QDs in a wide variety of strained semiconductor systems [4].

Thermodynamics and kinetics are both involved in the formation of self-assembled QDs. As illustrated in figure 1 for the case of III–V compounds semiconductors, In and As atoms deposited on a clean GaAs substrate held at high temperature, will self-assemble into smooth epitaxial atomic layers if the lattice mismatch between the material deposited and the substrate is not too large. The diffusion length of some of the group III elements deposited by MBE are sufficiently large to insure the layer by layer growth until a build up in the strain and surface energy of the epitaxial film switches the growth to the island mode. This change in the surface morphology is dictated by the minimization of the film energy.

The growth of self-assembled QDs is achieved by covering the smaller bandgap material of the islands with a wider bandgap epitaxial film (figure 1). The formation of a thin wetting layer is inherent to the process. The QDs' exact shape, dimensions and composition are not known accurately. In our samples, the size distribution of the QDs is controlled by the partially covered island (PCI) technique [5], in which, the growth sequence during the capping of InAs islands is modified by introducing growth interruptions. This technique reveals QDs with base diameters of 20–40 nm and heights of 4–6 nm having their ground state energy between 1.25 and 1.3 eV. We note that the majority of QDs have been observed to have ring-like shape in AFM studies. The optical properties that we discuss in this paper should not depend on the exact shape and structure since we do not apply magnetic fields [6]. The confinement energies for both electrons and holes in these QDs are larger than 100 meV. Energy separation between the ground and excited exciton (electron–hole) states typically exceeds 20 meV [7]. A random in plane distribution of islands is in general observed on the surface. The QD density of our samples can be made constant at 10^{10} cm^{-2} or with a gradient in density from zero to 10^{10} cm^{-2} in the In flow direction. These two different density profiles can be achieved by rotating or not rotating the wafer during the MBE growth, respectively.

The spectrum of a single QD is extremely rich. This richness arises primarily from the fact that the confinement length-scale is much larger than the lattice spacing, giving rise to multi-electron–hole excitations that differ in energy from the fundamental one by only a few millielectronvolts. The best known example is the biexciton line which appears when a photon is emitted from a QD containing two electrons and two holes, all in their ground motional states: the biexciton photon energy is red-shifted by about 3.5 meV in most InAs QDs due to Coulomb correlation effects [7–10]. For a weakly excited QD, the single-exciton (1X) line dominates the spectrum; increasing the excitation power results in the appearance of additional lines, most notably the biexciton line. Under non-resonant excitation, achieved by creating free-electron–hole pairs in GaAs, the number of electrons captured by the QD need not equal that of holes: in this case, charged exciton lines with small red or blue detuned emission energies may also appear in the spectrum. Finally, under strong excitation, the QD spectrum develops a strong background and is qualitatively different from the spectrum of a single atom.

Modern semiconductor nanofabrication allows the formation of sub-micron semiconductor structures with very smooth surfaces. Given the large index-of-refraction of semiconductors in general and GaAs in particular ($n \sim 3.5$), such structures can provide full three-dimensional confinement for optical modes, with mode volumes approaching the fundamental limit of $(\lambda/2n)^3$. Three types of nanostructures have been pursued in the context of QD cavity-QED: the micropillar structures obtained by etching a distributed Bragg reflector (DBR) cavity [11], microdisc structures [12, 13] and defects in 2D photonic crystals [14, 15]. In all three photonic structures, a GaAs layer containing InAs QDs is introduced during MBE growth to ensure that the QDs couple efficiently to the cavity mode at a location fixed by the growth. Figure 2 shows the SEM micrograph of a microdisc structure and a H2 defect in a 2D photonic crystal: both structures support high-Q cavity modes, with Q values exceeding 18 000 and 4000, respectively.

Different nano-cavity structures have certain advantages and disadvantages. Micropillar cavities appear to have Q values that are limited to $\sim$3000 for small mode volumes as

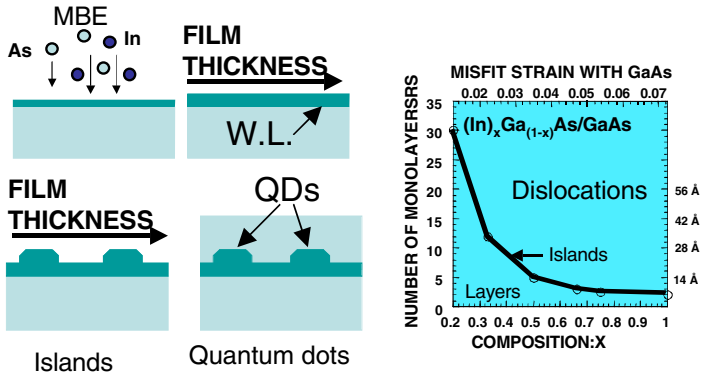

Figure 1. Schematic of the island growth process illustrated for the deposition of InAs on GaAs. Capping of the islands will transform the islands into QDs. An increase in the film thickness beyond the island formation stage will produce island coarsening and the introduction of misfit dislocations. The smaller bandgap material is shown in darker shading. The graph shows the critical thickness for island formation measured experimentally as a function of x the $In_xGa_{1-x}As$ layer composition.

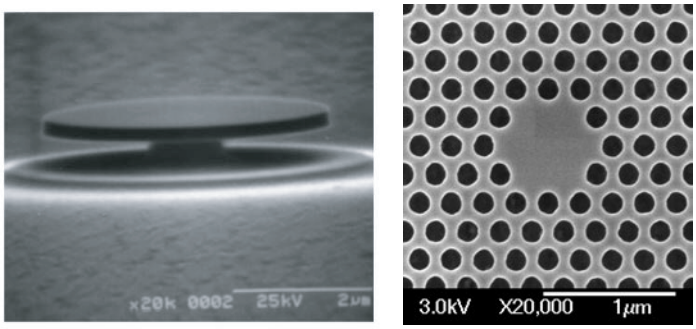

Figure 2. SEM pictures of the microdisc and 2D photonic crystal defect cavity structures. The microdisc structure has a diameter of 4.5 μm, with a corresponding cavity-mode volume of $V_{cav} \sim 200\ (\lambda/2n)^3$ (left). The highest Q values measured in this structure exceeded 18 000. The H2 defect in an otherwise perfect 2D photonic crystal with a lattice constant of 255 nm supports cavity modes with $V_{cav} \sim 20\ (\lambda/2n)^3$ and $Q = 4000$ (right).

$V_{cav} \sim 100\ (\lambda/2n)^3$ [11]. On the other hand, they provide highly directional output and easy coupling to optical fibre. Microdisc cavities can have $Q > 10\,000$ together with $V_{cav} \sim 50\ (\lambda/2n)^3$, but do not provide directional output [12, 13]. Photonic crystal defect cavities can have $Q \sim 2800$ and $V_{cav} \sim 4\ (\lambda/2n)^3$, or $Q \sim 4000$ for slightly larger cavities, in addition to providing directional output coupling [14, 15]. Photonic crystals also allow for the possibility of creating a quantum network of several nano-cavities linked by defect waveguides.

The most important achievement of QD cavity-QED to date has been the demonstration of the Purcell effect [16] in micropillar and microdisc structures. Gérard and co-workers [11] have used time-resolved photoluminescence (PL) techniques to measure the decay rate of an ensemble of QDs that resonantly couple to a $Q = 2250$ micropillar cavity mode with diameter $d = 1\ \mu$m. Their experimental results directly showed that the spontaneous emission rate of these resonant QDs is enhanced by a factor of five as compared to QDs that are out-of-resonance with the cavity mode. The measured value in these experiments is an average over many QDs and reflects the fact that the Purcell factors experienced by each QD are different. The Gérard group has also demonstrated similar spontaneous emission enhancement factors for an ensemble of QDs embedded in high-Q microdisc structures [12]. The typical QD density used in these experiments was 2×10^{11} cm^{-2}, which implies that approximately 2000 QDs were embedded in the cavity structure. Since the QDs had a large inhomogeneous broadening arising from size fluctuations, the actual (average) number of QDs that coupled resonantly to the cavity mode was around 20. Direct observation of the Purcell effect for a single QD in a microdisc cavity will be discussed in section 3.

3. A single quantum dot in a microdisc

Microdisc cavities support whispering gallery modes (WGMs) where photons are confined by total internal reflection within the disc circumference [17]. As noted in the previous section, WGMs can have high Q values with relatively small mode volumes ($Q = 12\,000$ for a 2 μm microdisc, $V_{cav} \approx 50\ (\lambda/2n)^3$ [18]), which in turn makes them suitable for cavity-QED studies despite the fact that they do not provide directional emission. WGM resonances are characterized by azimuthal (M) and radial (N) mode numbers, where M determines the azimuthal dependence $\exp(iM\phi)$ and $N - 1$ denotes the number of nodes in the radial direction. The modes exhibit a two-fold degeneracy due to the azimuthal dependence (M and $-M$). The WGMs with $N = 1$ are contained within a ring with an approximate width of $\lambda/2n$ [12]; for our microdisc structures only low radial number modes ($N = 1, 2, 3$) are observable since the post (with refractive index comparable to

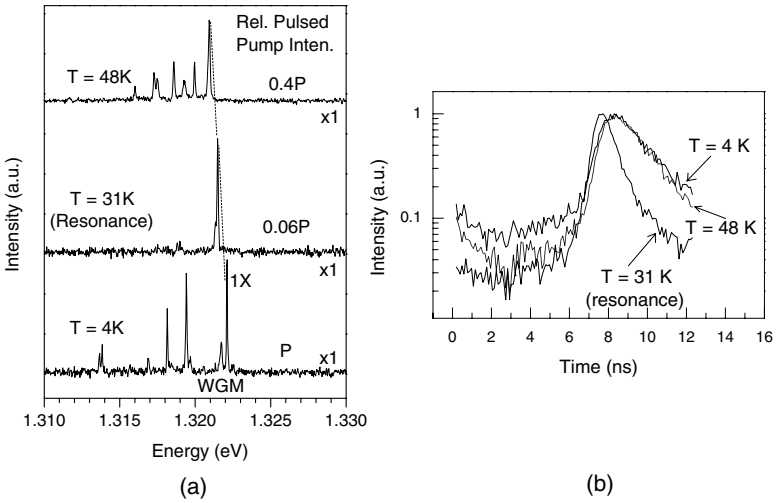

Figure 3. (a) PL spectra of a single InAs QD embedded in a 5 μm diameter microdisc taken at 4, 31 and 48 K under pulsed excitation at 790 nm (dashed curve is a guide for eye). (b) TCPC measurements on the single exciton (1X) emission: out of resonance with the WGM (4, 48 K), in resonance with the WGM (31 K) taken for pump intensities shown in (a).

that of the disc) provides large optical losses for high radial number WGMs.

We have analysed GaAs microdisc samples containing InAs QDs in the centre plane. First, a 0.5 μm $Al_{0.65}Ga_{0.35}As$ post layer was grown by MBE followed by the 200 nm GaAs disc layer. QDs were embedded in the centre plane of the 200 nm disc layer. The QD density of our sample was 2×10^6 cm^{-2}. Microdisc structures were then produced using a two-step wet-etching process [18, 19]. After defining circular patterns by photolithography, vertical etching was performed using an HBr based wet-etchant, followed by lateral etching using a dilute hydrofluoric acid (HF) solution that formed microdisc structures. The two-step wet-etching process was optimized to minimize the edge roughness, the limiting factor for the observed Q values. Following growth and processing, microdisc structures with diameters of 2–5 μm having only a few QDs randomly located in the centre plane were obtained.

In our experiments, we kept the sample in a He-flow cryostat (Oxford Ins., Microstat) allowing for temperature tuning between 4 and 300 K. We used a scanning optical microscope (NA = 0.55) for both collection and excitation in the normal direction. The QDs were excited using either a continuous wave (cw) diode laser (785 nm) or a mode-locked Ti:Sa laser (250 fs, 82 MHz, 790 nm) generating carriers in the GaAs buffer layer that are subsequently captured within a short timescale (<35 ps) [20]. Collected luminescence was detected by a spectrometer (spectral resolution 70 μeV) and a charge coupled device (CCD) detector for spectroscopy measurements. Lifetime measurements were performed using time-correlated single-photon counting (TCPC) where the pulsed laser emission and specific QD lines were sent to avalanche photodiodes (APDs) in a coincidence detection scheme [13]. For the results reported in this paper, narrowband interference filters (FWHM = 0.5 or 1 nm) were used in spectral filtering the single exciton (1X) emission. The output of the APD illuminated by the laser emission (1X emission) was sent to the start (stop) input of a time-to-amplitude converter whose output was stored in a multichannel analyser (MCA). The resulting histogram of coincidences in the MCA gives the population density function of the single exciton state of the QD in the limit where the reciprocal of the average counting rate is much larger than the measured time separation τ between photon pairs, which was always the case for our measurements. In the low excitation regime where our experiments were carried out, the biexciton emission or emission from the higher excited states were not observed. In this limit, the decay time in the coincidence histogram corresponds to the lifetime of the 1X transition [21].

We used temperature tuning to achieve coupling between a quantum dot single-excitonic transition and a WGM. Temperature tuning relies on the relatively stronger dependence of the 1X emission on temperature compared to the WGM, allowing a tuning range of ~3 meV between 4 and 50 K [13]. The temperature dependence of the energy of the WGM is due to the change in the refractive index of GaAs with temperature while the temperature dependence of the energy of the 1X transition is caused primarily by the changes in the bandgap energies. The observed temperature dependence is not inconsistent with a *Varshni's Law* approximation of the bandgap energies [22]. Figure 3(a) demonstrates the PL spectrum of the single QD located in a 5 μm diameter microdisc structure at three different temperatures, taken under nonresonant pulsed excitation conditions (790 nm). In the trace taken at 4 K, the resolution-limited peak at 1.3221 eV is identified as the single exciton recombination (1X) line, whereas the emission at 1.3218 eV (WGM) is due to background emission that is coupled to a WGM. The 1X line is identified by power-dependent PL experiments (figure 4) as well as photon antibunching measurements (data not shown), while the WGM line is identified by the power-dependent PL spectra, and its relatively large linewidth. As we discuss in the next paragraph, the existence of a resonant coupling between the 1X and WGM lines is further proof for the identification of the WGM emission. The linewidth of the WGM, 160 μeV, corresponds to a Q value of 8300. We note that the source of the WGM radiation at 4 K is not clearly identified; it might be caused by the residual emission from the GaAs disc, or by the emission from the QD. There

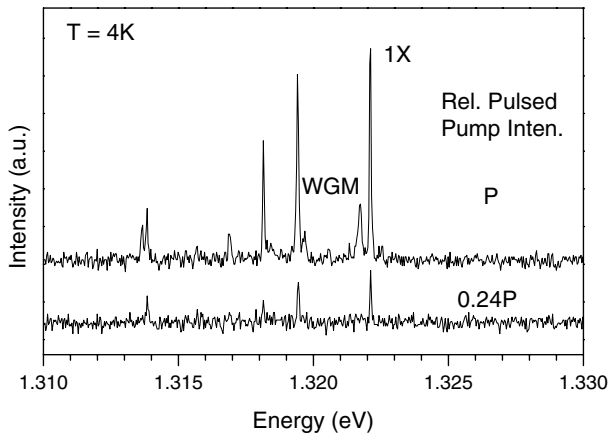

Figure 4. PL spectra of the single InAs QD analysed in figure 3, taken at 4 K under relative pulsed pump intensities 0.24 P and P. Contributions from the excitonic ground state transition (1X), and higher excited states (e.g. biexciton, charged exciton) are visible in both of the spectra while a WGM is only visible in the spectrum taken under high excitation power (P).

is an indication supporting the latter: in microdisc cavities that do not contain any QDs, we have not observed WGM luminescence in photon energies 1.25–1.35 eV (bulk QD emission region) even though we observed WGMs coupled to the wetting layer luminescence (1.44 eV). Contributions from other charged excitonic emissions are also visible in figure 3(a) [23].

Figure 3(b) demonstrates TCPC experiments performed for the power levels and temperatures indicated in figure 3(a). These measurements were taken under low excitation conditions where the biexciton emission or emission from the higher excited states were negligible. Identical decay times of 1.8 ns at 4 and 48 K show that when the 1X transition is not coupled to any WGMs, its lifetime has no dependence on temperature between 4 and 48 K. Hence, nonradiative recombination does not significantly effect the dynamics of the 1X transition within this temperature range. When the 1X emission is in resonance with the WGM at 31 K, the decay time is reduced to 850 ps, leading to the observation of a Purcell factor of at least two. The background coupled to the WGM at 4 K has a negligible contribution to the observed decay time at 31 K due to the low pumping power (0.06 P) used in the experiment. The negligible coupling of background to the WGM radiation is also observable in figure 4 where we plot the PL spectra for two different pump power intensities at 4 K.

We note here that the electron–hole pairs in the wetting layer have average recombination times of ∼300 ps [24] or larger depending on the existence and nature of trap states. For our low-density QD samples, we measured lifetimes as long as 1 ns on the low-energy side of the wetting layer luminescence using the TCPC technique. Hence, the measured decay time at 31 K in our case may be limited by the lifetime of the wetting layer states that pump the QD. For our specific WGM ($Q = 8300$, $V_{cav} \sim 240\ (\lambda/2n)^3$), an ideal Purcell effect of $F_P = 22$ [12] is estimated assuming an ideal spatial match between the QD and WGM.

Besides providing an enhancement in the radiative recombination rate, the Purcell effect also ensures that photons are primarily emitted into a specific cavity mode. These properties are important for realizing fast and efficient semiconductor light sources. In particular, for a triggered single-QD single-photon source [25–27], the Purcell effect is crucial. A QD can provide an almost deterministic stream of single-photon pulses, if and only if the emitted photons are collected with a high probability: without the Purcell effect, collection efficiency from a single QD would be less than 10%, due to the large index of refraction of semiconductors. Even though microdisc cavities allow for large Purcell factors and can ensure that the photons are primarily emitted into a specific WGM, they cannot improve the overall collection efficiency significantly due to non-directional output from the WGMs.

4. Photonic crystal defect cavities

2D photonic crystal defect cavities provide ideal structures for photon confinement and manipulation. In these structures, a 2D photonic crystal provides the in-plane optical confinement while index guiding is used to achieve confinement in the vertical direction (figure 2). Using the analogy which is often made with electronic crystals, the 2D 'photonic lattice' creates a forbidden gap in the dispersion relation for in-plane propagation of light. The defect plays the role of a donor atom by creating one or more states which lie inside the photonic bandgap; these are the resonant modes of the cavity [28]. Utilizing a photonic bandgap creates the possibility for stronger optical confinement than is possible in microdiscs, so photonic crystal defect cavities are capable of much smaller mode volumes (up to 25 times smaller). Photonic crystal defect cavities have the added benefit that errors introduced during the fabrication process can automatically lift degeneracies while still allowing high-Q modes. Since these cavities are formed by a defect in a much larger periodic structure, they offer the prospect of a variety of coupled cavity designs, which would allow the creation of quantum networks.

We have fabricated 2D photonic crystal defect cavities in GaAs membranes with lattice constants as small as 255 nm. The starting material consisted of five layers of MBE-grown InAs 'self-assembled' QDs, which were embedded within 180 nm of GaAs to form the 'active layer' of the structure. The QDs were grown with a density of 100 QDs μm^{-2}/layer. A 500 nm $Al_{0.2}Ga_{0.8}As$ layer serves as a 'sacrificial layer'; when etched, it will allow the formation of a photonic crystal membrane. The fabrication consists of a four-step process which makes use of electron-beam lithography, reactive ion etching (RIE) and a chemical wet etch for lift-off. We used a JEOL JBX-5DII(U) electron-beam lithography tool to write a triangular lattice of circles in 100 nm of resist. The pattern was transferred from the resist to a PECVD-deposited layer of SiN, because the nitride is a more durable etch mask in the subsequent processing. We were able to achieve an etch selectivity of 2 to 1 when transferring a photonic crystal pattern of 150 nm holes to 100 nm of SiN by RIE in 20 sccm CHF_3 at 10 mT and 250 V. Following this step, the residual resist was removed, and the pattern was transferred from SiN to GaAs by RIE in 10 sccm $SiCl_4$ at 3 mT and 100 W. The final step was to remove the AlGaAs sacrificial layer by making use of the high selectivity of HF to create a thin photonic crystal membrane. The etch was timed to control the degree of undercut so that approximately a 10 μm region surrounding the defect cavity

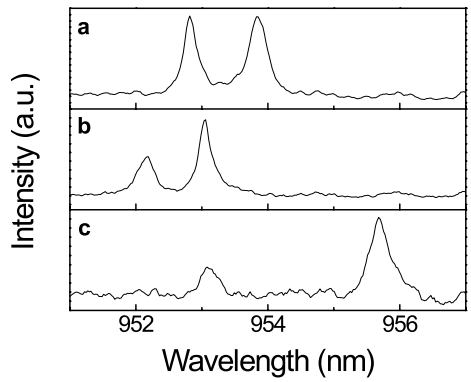

Figure 5. Measured PL spectra of two high-Q modes for H2 cavities on the same sample. The observed Q values are: (a) 4000 and 3000, (b) 3000 and 3800 and (c) 1900 and 2700.

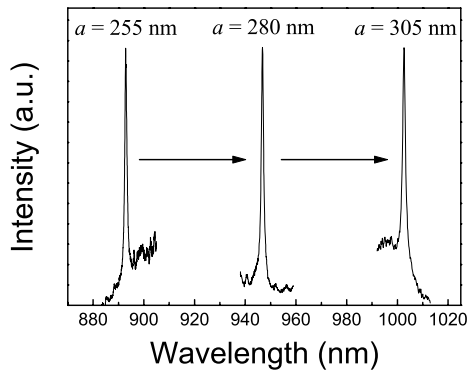

Figure 6. Measured PL spectra for H2 cavities with lattice constants (a) 255, (b) 280 and (c) 305 nm. The cavity mode shifts from 893, to 948 and to 1002 nm with increasing lattice constant.

was released from the substrate. The fully processed photonic crystal defect cavity is shown in figure 2.

Recent progress in photonic crystal defect cavities has resulted in coupling performance competitive with the best results in microdiscs. We used the inhomogeneously broadened spectrum from a high density of QDs embedded in the defect to probe the resonant modes of defect cavities. The low-temperature spatially resolved PL measurement is the same experiment described in section 3. Figures 5(a)–(c) show PL from several equivalent H2 defect cavities having a lattice constant of 255 nm, and the same two modes are observed for all cavities shown. The cavity modes at 952.8 and 953.9 nm in figure 5(a) were fit to Lorentzians giving linewidths of 330 and 440 μeV, corresponding to Q values of 4000 and 3000, respectively [14]. Using an estimate for the mode volume of 20 $(\lambda/2n)^3$ suggests the Purcell factor in these defect cavities can be as high as 120.

The peaks in figures 5(a)–(c) are too closely spaced to constitute different order eigenmodes of the cavity. On the other hand, we expect from the C_{6v} symmetry of these cavities, some of the eigenmodes will be doubly degenerate. In the actual cavities measured, there are a large number of fabrication 'errors' (nonuniformity in the size, shape and placement of etched holes) which might be responsible for compromising the symmetry of the structures, and hence for removing the degeneracy of the eigenmodes. This suggests that the two distinct, high-Q modes shown in figures 5(a)–(c)

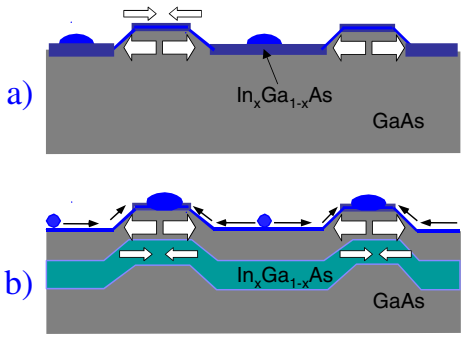

Figure 7. Schematics of two possible configurations for controlled nucleation on a mesa patterned substrate. In (a), the strain distribution in the structure is illustrated by arrows and the crystal growth will preferentially occur in the valleys. In (b), a coherently strained InGaAs stressor layer is used to enhance the strain on the mesa edge tops. The growth of islands will preferentially occur on the mesa tops where the strain build up is the largest.

are symmetry-degenerate modes which have been split by the perturbation related to these fabrication 'errors'. It is important to recognize this degeneracy has been lifted without any change to the microcavity design while at the same time the Q value remains high. However, if the splitting of the mode degeneracy results from fabrication imperfections, then we are constrained by a very delicate balance between achieving high-Q modes with a reasonable splitting. By utilizing this inherent property of photonic crystal defect cavities, we would ultimately be able to couple the emission of a QD to a single cavity mode.

In order to obtain spectral coupling, the optical modes of the cavity should be tunable in the wavelength range of the QDs by the choice of suitable design parameters. In a 2D photonic crystal defect cavity, the critical parameters are the hole radius r lattice constant a and membrane thickness t. The parameters r, a and t, can be adjusted to tune the energies of the cavity modes, and we can vary the hole radius r and lattice constant a over a wide range for different cavities on the same sample. Figure 6 shows PL measurements for H2 defect cavities having lattice constants of 255, 280 and 305 nm. As the lattice constant was increased, the cavity resonance shifted from 893, to 948 and to 1002 nm. This demonstrates that we need only adjust the lattice constant a of our defect cavity to obtain spectral coupling in the desired wavelength range.

Photonic crystal defect cavities offer new prospects for quantum dot cavity-QED. The measured cavity Q factors we have obtained demonstrate that these structures are already suitable for device applications in the weak coupling regime. Photonic crystals offer a very rich parameter space that we have only begun to investigate, and much may yet be done to obtain even larger Purcell factors. In the future, we may discover new cavity configurations with an even better combination of high-Q and small mode volume to achieve the much heralded strong coupling between a single QD and a nondegenerate optical mode [29].

5. Control of quantum dot nucleation

If the emitter is not located at the cavity field maximum, the radiative decay rate enhancement that we observe in practice will be small. The next-generation of QD microcavity devices

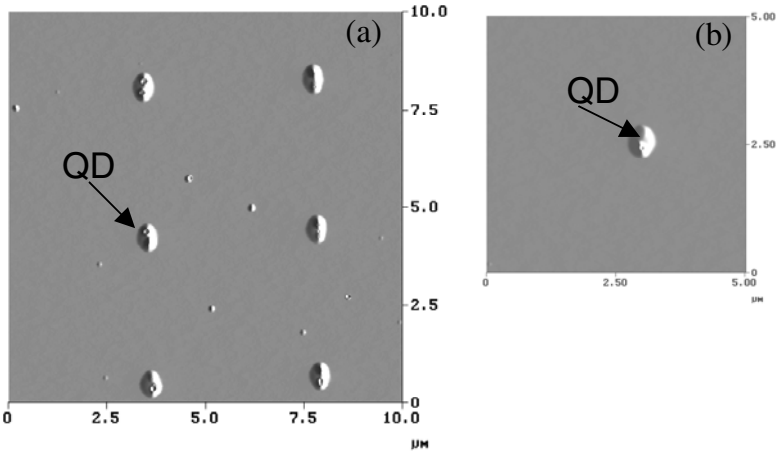

Figure 8. AFM pictures of the GaAs {100} surface with surface depressions after a GaAs buffer layer regrowth and an InAs thin-layer deposition. In (a) the In flux was adjusted to grow between one and three InAs islands per depression. In (b), low In flux deposition and the statistical distribution of In allows the formation of a single InAs island in some of the depressions.

would benefit greatly from the controlled positioning and ordering of QDs. Controlling the island nucleation can be achieved through several techniques. The first method uses the directed migration of adatoms to a concave surface area. This can be realized by engineering the surface chemical potential [30, 31] using a patterned surface (figure 7(a)).

The chemical potential lowering due to capillarity effects will induce a driving force for adatom diffusion towards the concave centres and trigger island nucleation before the critical thickness for islanding is reached in other parts of the surface. A demonstration of the technique is shown in the AFM pictures in figure 8. The QDs are nucleated only within the surface depressions. The periodicity between the surface depressions formed by e-beam lithography prior to the InAs deposition is 4 μm. The InAs islands are found to form only in the surface depressions. The measured In surface diffusion using this technique is $\approx$15 μm.

In this method, the long diffusion length of In and the surface strain relieving process induce the InAs islands nucleation in the valleys on the GaAs surface. On the other hand, the thermodynamics and diffusion kinetics can be changed by introducing a local strain field on the surface. As shown in figure 7(b), this can be achieved by growing a coherently strained film of InGaAs below the surface. In this case, the InAs film will grow more rapidly on the mesa tops and induce a preferential growth on InAs islands on top of the subsurface stressors [4]. A patterned substrate composed of an ordered lattice of mesas is fabricated using an optical holographic process on a GaAs surface. The InGaAs islands are deposited by MBE [4]. Figure 9 shows examples of two QD lattices formed by deposition of InAs on the mesa ridges of a prepatterned substrate. The two types of mesa lattices promote the formation of InAs islands on the mesa tops. The number of islands in the lattice basis was found to depend on the mesa shape and width and on the In flux.

Finally, we note that a good control over the mesa shapes should promote the formation of a narrower size distribution for the islands. Under optimal conditions and for a pyramid-shaped mesa, it could be possible to form lattices with one island per mesa.

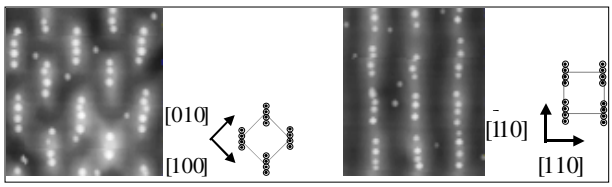

Figure 9. Examples of ordered InAs island lattices [4]. The InAs islands are deposited on a GaAs patterned substrate and the schematic of the unit cell of these two lattices correspond to each of the atomic force micrographs. The mesa ridges defined by holographic exposure of a photoresist and etching have different crystal orientations. The lattice parameter is $\approx$250 nm.

6. Aligning quantum dots with photonic nanostructures

As was previously mentioned, photonic crystal defect cavities have the advantage of providing small mode volumes, $V_{cav} \sim 2\,(\lambda/2n)^3$ while still demonstrating high Q (a few thousand). The small modal volume and the resulting reduced number of QDs within the cavity provide considerable challenges to achieving strong coupling between the cavity modes and the QDs. Our successful photonic crystal cavities have incorporated $\sim$500 QD μm^{-2}. On a given sample, it is always most difficult to observe QD–cavity coupling in the smallest volume H1 cavities. In these structures, less than 50 QDs would be included within the geometric boundaries of the photonic crystal cavity; the existing dispersion in QD size and placement makes it difficult to achieve the necessary coincidence of QD and modal frequency, as well as QD location at antinodes of the mode.

Ideally, we would selectively nucleate QDs to be formed at the expected antinodes of the cavity, and subsequently form the cavity 'around the QDs'. Patterning of the substrate surface prior to QD growth to achieve variation in surface topography and or/strain can result in some selective formation of self-assembled QDs. The previous section of this paper described the use of a periodic subsurface stressor lattice to form QDs into a QD lattice [32]. Such techniques may also result in better control of the *variation in size* (hence frequency) of the QDs. If the starting material for the cavity were then to

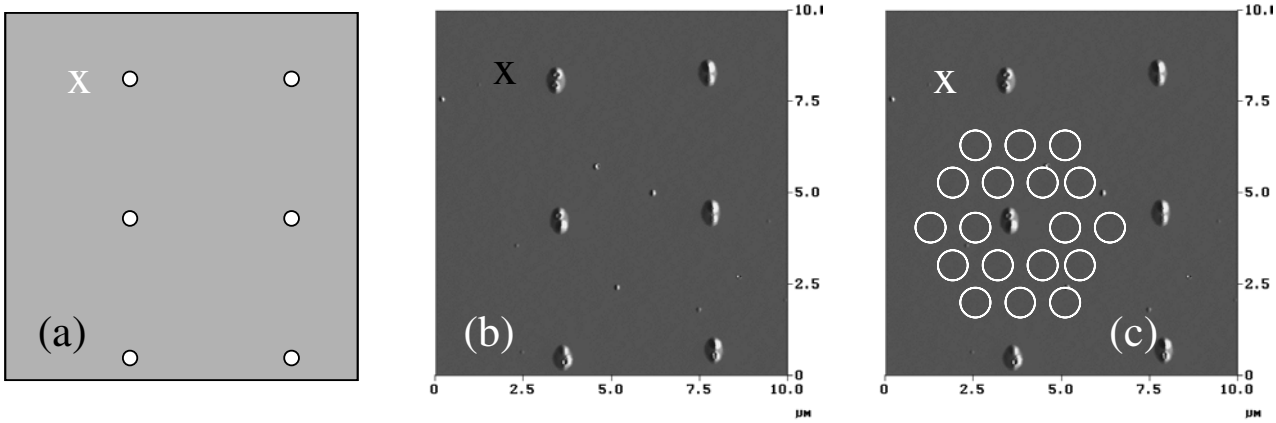

Figure 10. Formation of QDs aligned within photonic crystal cavities. (a) Electron beam delineation of nucleation sites. (b) Sample after growth of QDs, and (c) aligned electron beam patterning of photonic crystal cavity.

appear as in figure 8, one could subsequently form a photonic crystal cavity 'around' the QDs, as indicated schematically in figure 10. A major challenge would be the accurate alignment of the sub-micron dimensioned, electron beam-written cavity with respect to the position of the QDs. Electron beam lithography and subsequent pattern transfer would be used to define regions on the substrate where nucleation of the QDs would take place. Alignment marks defined with the first e-beam lithography would have to preserve their high contrast throughout the subsequent QD growth process, while at the same time not compromising the quality of the MBE growth of the dots. Alignment accuracy better than a few tens of nanometres is needed to ensure that the subsequent electron beam-written photonic crystal structures are correctly positioned about the QD locations. We are in the process of developing and evaluating various alignment schemes and processes.

7. Outlook

The principal factors that limit QD cavity-QED are the spatial and spectral overlap of QD resonances with high-Q cavity modes. The technique discussed in the previous section is likely to solve the spatial overlap problem in the near future. The spectral overlap, however, is more tricky due to the poor control we have over QD and cavity resonance energies. The temperature tuning technique discussed in section 3 is far from optimal, since increasing the sample temperature enhances the dipole dephasing rate [33], potentially prohibiting the observation of the strong coupling regime. Utilization of the ac-Stark effect induced on the QD fundamental exciton transition by a red-detuned laser field on the other hand, could provide a dephasing-free method to tune QDs into resonance with high-Q cavity modes. It must be stated, however, that the uncertainty in QD energies is typically much larger than the tuning range available with either of these techniques, which in turn implies that several QDs need to be placed inside the cavity mode to ensure that one of them could be tuned into resonance. Control of QD exciton energies during growth would certainly constitute a breakthrough for cavity-QED experiments. Techniques for tuning the cavity-mode energy independently of the QD resonance also need to be explored.

Is QD cavity-QED useful for QIP? Since conduction band electron spins are known to have long coherence times in two- or three-dimensional semiconductors, the most obvious way to implement QIP is to define the spin of an excess electron in a QD as a qubit. It has been shown that cavity-assisted spin-flip Raman transitions enabled by high-Q microcavity modes can be used to implement all-optical QIP based on QD spins [34]. Good-cavity limit of cavity-QED where $g^2 > \Gamma_{cav}\Gamma_{deph}$ is essential for the implementation of the scheme proposed in [34]. We note that good-cavity limit is easier to attain than the strong-coupling regime; we expect this to be the case for photonic crystal defect cavities with ultra-small mode volumes, but relatively fast Γ_{cav}.

A qualitatively different method for utilizing QDs in QIP is in triggered single-photon generation. A significant fraction of early key experiments in the field of quantum information, such as quantum key distribution and quantum teleportation, have been carried out using photons and linear optical elements such as polarizers and beam splitters. However, it was generally believed that the role of linear optics in QIP was limited to these specific applications, due to the difficulty in implementing conditional quantum dynamics using single photons. In contrast, the recent work of Knill *et al* [35] demonstrated that efficient quantum computation is possible using linear optics.

The principal requirement for linear optics quantum computation (LOQC) is the presence of a single-photon source that generates indistinguishable photons. This can be achieved only if the generated photons are Fourier-transform limited, which is in turn guaranteed if the fundamental exciton transition is broadened predominantly by spontaneous emission. Experiments on InAs QDs embedded in bulk semiconductors demonstrated that the linewidth is at most twice as large as that of radiative broadening [33]. Enhancement of the radiative decay by the Purcell effect could then ensure that the generated photons are transform limited. A second important requirement for LOQC is the high-efficiency (>99%) of the single-photon source: while this is a very demanding requirement, the only way to meet it would be to use directional output from a cavity that one could obtain using

a large Purcell effect. Recently, Santori and co-workers [36] have realized a source that generates nearly transform-limited single-photon pulses, and used this source to demonstrate two-photon interference. This experiment provides direct evidence for the indistinguishability of single photons generated by a single QD, highlighting the potential of QD cavity-QED for applications in LOQC.

Acknowledgments

The authors would like to thank Drs C Becher and P Michler for their contributions to this work. They also acknowledge financial support from the Humboldt foundation (AI), Packard Foundation, and ARO.

References

[1] Haroche S and Kleppner D 1989 *Phys. Today* **42** 24
[2] Turchette Q A, Hood C J, Lange W, Mabuchi H and Kimble H J 1995 *Phys. Rev. Lett.* **75** 4710
[3] Rauschenbeutel A, Nogues G, Osnaghi S, Bertet P, Brune M, Raimond J-M and Haroche S 2000 *Science* **288** 2024
[4] Petroff P M, Lorke A and Imamoğlu A 2001 *Phys. Today* **54** 46
[5] Garcia J M, Mankad T, Holtz P O, Wellman P J and Petroff P M 1998 *Appl. Phys. Lett.* **72** 3172
Garcia J M, Medeiros-Ribeiro G, Schmidt K, Ngo T, Feng J L, Lorke A, Kotthaus J and Petroff P M 1997 *Appl. Phys. Lett.* **71** 2014
[6] Lorke A, Luyken R J, Govorov A O, Kotthaus J P, Garcia J M and Petroff P M 2000 *Phys. Rev. Lett.* **84** 2223
[7] Zrenner A 2000 *J. Chem. Phys.* **112** 7790
[8] Gammon D, Snow E S, Shanabrook B V, Katzer D S and Park D 1996 *Science* **273** 87
[9] Zrenner A, Butov L V, Hagn M, Abstreiter G, Böhm G and Weimann G 1994 *Phys. Rev. Lett.* **72** 3382
[10] Dekel E, Gershoni D, Ehrenfreund E, Spektor D, Garcia J M and Petroff P M 1998 *Phys. Rev. Lett.* **80** 4991
[11] Gérard J-M, Sermage B, Gayral B, Legrand B, Costard E and Thierry-Meig V 1998 *Phys. Rev. Lett.* **81** 1110
[12] Gérard J-M and Gayral B 1999 *J. Lightwave Technol.* **17** 2089–95
[13] Kiraz A, Michler P, Becher C, Zhang L, Hu E, Schoenfeld W V, Petroff P M and Imamoğlu A 2001 *Appl. Phys. Lett.* **78** 3932
[14] Reese C, Gayral B, Gerardot B D, Imamoğlu A, Petroff P M and Hu E 2001 *J. Vac. Sci. Technol.* B **19** 2749
[15] Yoshie T, Vučković J and Scherer A 2001 *Appl. Phys. Lett.* **79** 4289
[16] Purcell E M 1946 *Phys. Rev.* **69** 681
[17] McCall S L, Levi A F J, Slusher R E, Pearton S J and Logan R A 1992 *Appl. Phys. Lett.* **60** 289
[18] Gayral B, Gérard J-M, Lemaître A, Dupuis C, Manin L and Pelouard J L 1999 *Appl. Phys. Lett.* **75** 1908
[19] Michler P, Kiraz A, Zhang L, Becher C, Hu E and Imamoğlu A 2000 *Appl. Phys. Lett.* **77** 184
[20] Raymond S, Fafard S, Poole P J, Wojs A, Hawrylak P, Charbonneau S, Leonard D, Leon R, Petroff P M and Merz J L 1996 *Phys. Rev.* B **54** 11548
[21] Bacher G, Weigand R, Seufert J, Kulakovskii V D, Gippius N A, Forchel A, Leonardi K and Hommel D 1999 *Phys. Rev. Lett.* **83** 4417
[22] Palankovski V 2000 *PhD Thesis* http://www.iue.tuwien.ac.at/publications/PhD%20Theses/palankovski
[23] Kiraz A, Fälth S, Becher C, Gayral B, Schoenfeld W V, Petroff P M, Zhang L, Hu E and Imamoğlu A 2002 *Phys. Rev.* B **65** 161303(R)
[24] Raymond S, Hinzer K, Fafard S and Merz J L 2000 *Phys. Rev.* B **61** 16331
[25] Imamoğlu A and Yamamoto Y 1994 *Phys. Rev. Lett.* **72** 210
[26] Michler P, Kiraz A, Becher C, Schoenfeld W V, Petroff P M, Zhang L, Hu E and Imamoğlu A 2000 *Science* **290** 282
[27] Solomon G S, Pelton M and Yamamoto Y 2001 *Phys. Rev. Lett.* **86** 3903
[28] Yablonovitch E 1994 *J. Mod. Opt.* **41** 173
[29] Vučković J, Lončar M, Mabuchi H and Scherer A 2001 *Phys. Rev.* E **65** 016608
[30] Mui D S, Leonard D, Coldren L A and Petroff P M 1995 *Appl. Phys. Lett.* **66** 1620
[31] Jeppesen S, Miller M S, Hessman D, Kowalski B, Maximov I and Samuelson L 1996 *Appl. Phys. Lett.* **68** 2228
[32] Lee H, Johnson J A, He M Y, Speck J S and Petroff P M 2001 *Appl. Phys. Lett.* **78** 105
[33] Bayer M and Forchel A 2002 *Phys. Rev.* B **65** 041308
[34] Imamoğlu A, Awschalom D D, Burkard G, DiVincenzo D P, Loss D, Sherwin M and Small A 1999 *Phys. Rev. Lett.* **83** 4204
[35] Knill E, Laflamme R and Milburn G 2001 *Nature* **409** 46
[36] Santori C, Fattal D, Vučković J, Solomon G S and Yamamoto Y 2002 *Nature* **419** 594